ELSEVIER

Magnetic Resonance Materials in Physics, Biology and Medicine 13 (2002) 177–185

MAGMA
Magnetic Resonance Materials in Physics, Biology and Medicine

www.elsevier.com/locate/magma

A desktop magnetic resonance imaging system

Steven M. Wright [a,*], David G. Brown [a], Jay R. Porter [b], David C. Spence [a], Emilio Esparza [c], David C. Cole [c], F. Russell Huson [c]

[a] *Department of Electrical Engineering, Zachry Engineering Center, Texas A & M University, TAMU 3128, College Station, TX 77843, USA*
[b] *Department of Engineering Technology, Texas A & M University, TAMU 3128, College Station, TX 77843, USA*
[c] *Department of Physics, Texas A & M University, TAMU 3128, College Station, TX 77843, USA*

Received 20 August 2001; received in revised form 28 September 2001; accepted 9 October 2001

Abstract

Modern magnetic resonance imaging (MRI) systems consist of several complex, high cost subsystems. The cost and complexity of these systems often makes them impractical for use as routine laboratory instruments, limiting their use to hospitals and dedicated laboratories. However, advances in the consumer electronics industry have led to the widespread availability of inexpensive radio-frequency integrated circuits with exceptional abilities. We have developed a small, low-cost MR system derived from these new components. When combined with inexpensive desktop magnets, this type of MR scanner has the promise of becoming standard laboratory equipment for both research and education. This paper describes the development of a prototype desktop MR scanner utilizing a 0.21 T permanent magnet with an imaging region of approximately 2 cm diameter. The system uses commercially available components where possible and is programmed in LabVIEW software. Results from 3D data sets of resolution phantoms and fixed, newborn mice demonstrate the capability of this system to obtain useful images from a system constructed for approximately $13 500.

Keywords: MRI; Microscopy; Instrumentation; Spectrometer; Radiofrequency; Magnet

1. Introduction

There has been a great deal of interest recently in developing techniques for imaging small animals [1]. High field systems provide outstanding image quality with high resolution and reasonable imaging times, but can be prohibitively expensive for screening large numbers of animals. A number of groups are working to develop low-cost magnetic resonance imaging (MRI) systems with imaging regions from whole-body down to the cellular level [2–7]. Widespread use of miniature MRI systems will require lowering the cost and complexity typically associated with clinical MRI. Progress is being made in low-cost, light weight magnet technology, microcoils, and spectrometer design, and low-cost, desktop MRI systems for a variety of applications now appear to be a reasonable goal [7–16]. This paper describes a PC based desktop scanner built at Texas A&M for approximately $13 500 in hardware costs, including a 0.21 T, C-shaped permanent magnet with a 2.5 cm imaging region. The initial goal in building the desktop transceiver was to develop a low-cost MR system capable of high resolution imaging of small volumes on compact, low-field MR magnets. The eventual goal is to be able to image samples with volumes of 1 $in.^3$ (16.4 ml) or less, at field strengths of 0.25 T or less, with a target resolution of $75 \times 75 \times 200$ μm.

2. Methods

The entire system, including the magnet, was constructed in the Magnetic Resonance Systems Lab at Texas A&M. The following sections briefly describe the magnet, transceiver and software.

* Corresponding author. Tel.: +1-979-845-9413; fax: +1-979-845-6259.
E-mail address: wright@ee.tamu.edu (S.M. Wright).

1352-8661/02/$ - see front matter
PII: S1352-8661(01)00147-8

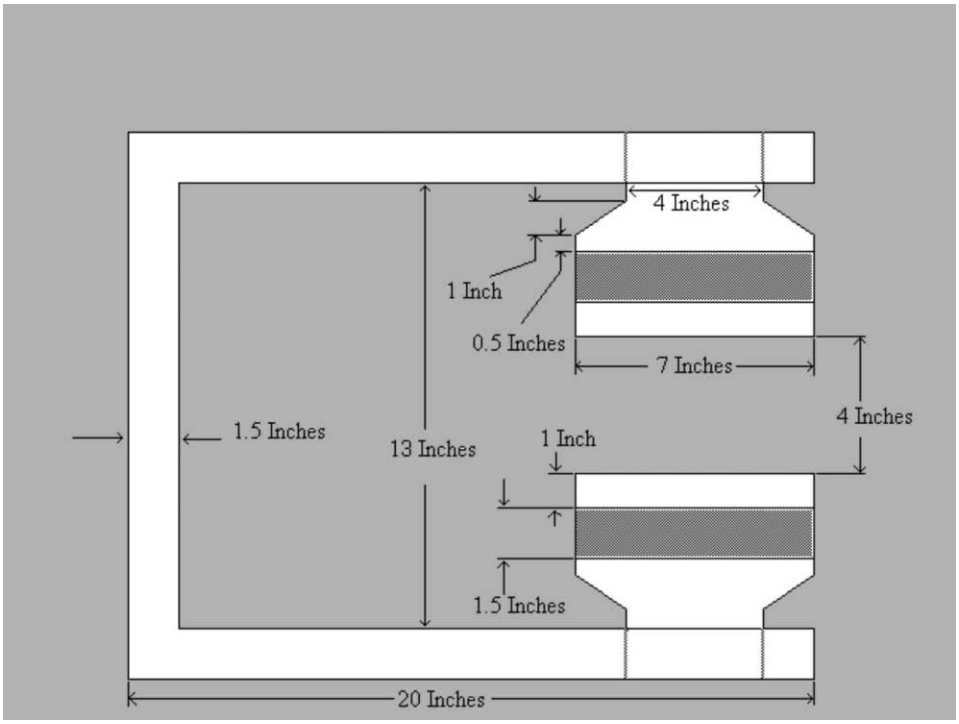

Fig. 1. Drawing of the C-shaped permanent magnet used for the desktop scanner. The 13 inch gap between the C-arm was covered with an additional metal plate for additional rigidity.

2.1. Magnet

The magnet design has been described elsewhere in some detail [13,14] and will only be summarized here. A C-shape design, shown in Fig. 1, was chosen, with a target field of 0.22 T and a 5 cm homogeneous region. The C-gap is 10 cm and the pole diameter is 17.5 cm. The magnet poles were constructed using 330 pieces of NdFeB material in $1 \times 1 \times 0.5$ in.^{3} blocks. Each block was numbered, and the energy measured. The magnets were then stacked in groups of three in order to minimize energy variation. This resulted in several groups of magnetization energy, which were then placed symmetrically around the pole pieces. The pole pieces were designed using the 2D Pandira code from Los Alamos National Lab. After shimming by adjustment of the pole pieces and with four electrical shim coils, a half-height linewidth of ~ 150 Hz at 8.96 MHz was obtained (~ 20 ppm) at 0.21 T from a cylindrical phantom 0.75 in. long by 0.55 in. in diameter. Total material cost was \$2500 for the NdFeB pieces and \$800 for additional steel. The magnet is shown in Fig. 2, with a prototype gradient set between the pole pieces.

2.2. Spectrometer

The dynamic range required at the RF front end of the receiver was determined by assuming a 3 cm diameter, five-turn solenoid RF coil with a Q of 100 and a mouse sized (1 in. diameter, 1 in. long) cylindrical water phantom. From standard MR equations, the noise level in a 100 kHz bandwidth at room temperature was calculated to be approximately 0.04 μV (-135 dB m), and the maximum signal as 67.5 μV (-70.4 dB m). Thus, detecting an MR signal in these conditions would require a receiver with a minimum dynamic range of 64.6 dB. A block diagram of the transceiver is shown in Fig. 3 while the completed spectrometer appears in Fig. 4. In Fig. 3, the dashed lines indicate control signals and the solid lines MR signals. Each block is briefly described below.

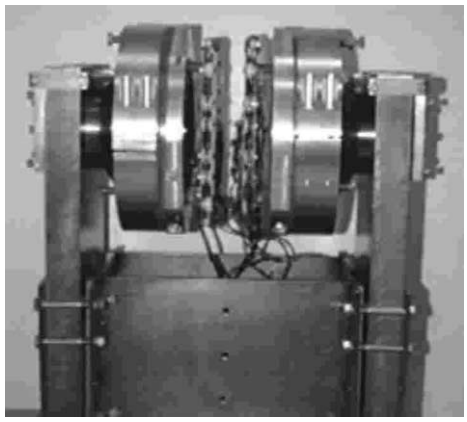

Fig. 2. Photograph of the final C-shaped, desktop magnet. A prototype, wire-wound planar gradient set is between the poles. Mechanical shimming is performed by adjusting the screws seen on the outside of both pole pieces.

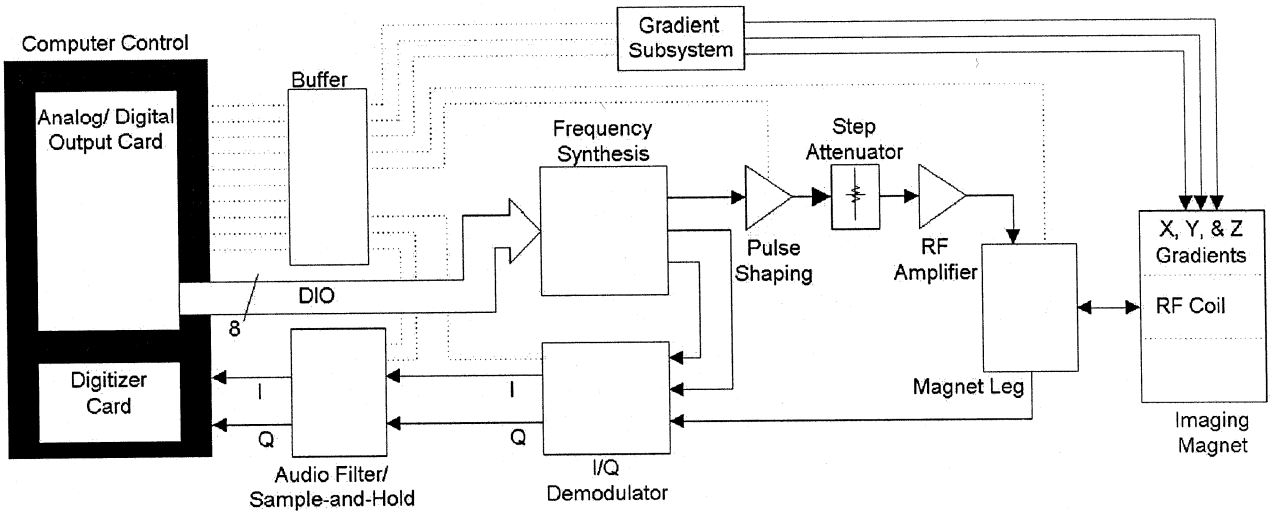

Fig. 3. Block diagram of the spectrometer.

A standard Pentium-II, 300 MHz PC with 128 MB of RAM was used to control the system. The analog input and output and digital control functions were done with standard PCI-bus boards from National Instruments (Austin, TX). All software for running the transceiver was written in National Instruments LabVIEW.

The gradient amplifiers use LM12 high power op-amps from National Semiconductor (Santa Clara, CA), which are able to drive ± 10 A. The final gradient amplifier circuit is based on a current amplifier, shown in the LM12 data sheet, that was modified by adding DC offset and gain controls. Gradient filters were implemented with commonly available 20 A, 60 Hz EMI power line filters. A standard planar gradient coil set [17] was designed for a 1 in. field-of-view with a sensitivity of 0.45 G/cm/A, and then etched on six, 8 oz. copper clad PC boards.

The frequency synthesis block consists of three DDS circuits which generate the RF transmit frequency and local oscillator signals for demodulation of the received MR signal. The DDS circuits are built around Harris HSP45102 and HI5735 integrated circuits (Intersil, Irvine CA). The HSP45102 is a numerically controlled oscillator (NCO) which provides a 12 bit binary sine wave output. The HI5735 is a 12 bit, high speed digital to analog converter (DAC) with a maximum throughput rate of 80 MSPS. Together, these two chips form a waveform synthesis circuit capable of generating 0–20 MHz sine waves with 0.009 Hz of digital tuning resolution. The output phase of the generated waveforms is controllable in 90° increments. RF pulse shaping was accomplished with a National Semiconductor CLC5523, a single chip, wideband, variable gain amplifier. The amplifier gain may be varied from 0 to -80 dB at rates up to 4 dB/ns by application of an external modulation signal. The CLC5523 is used in conjunction with a step attenuator to allow further control over transmit power levels.

For the final RF amplifier in the transmit side, there are a wide variety of low-cost, linear amplifiers available which operate from 1.8–30 MHz. A model 20B 20 W amplifier from Henry Radio (Los Angeles, CA) was used, which provided more than sufficient power for the 1 in. field-of-view. Because this amplifier was not blanked, an external PIN diode blanking switch was added.

The magnet leg houses the RF amplifier blanking switch, a passive T/R switch, and the first two stages of low-noise gain and filtering for the receiver. For the initial gain stage of the receiver a Miteq model AU-1519-7480 low-noise preamplifier was used (Miteq, Inc., Hauppage, NY). The amplifier provides 60 dB gain

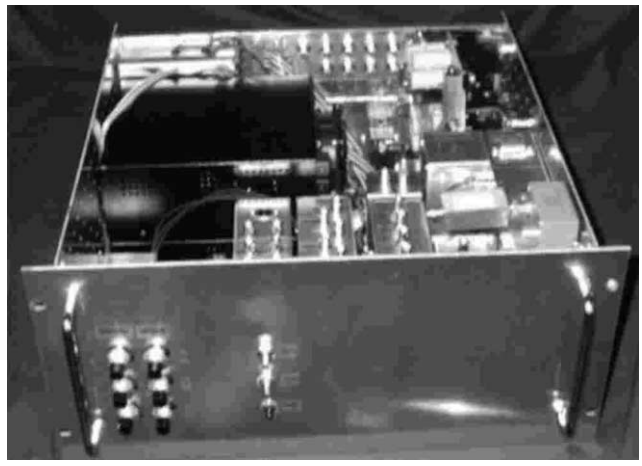

Fig. 4. View of the completed spectrometer. The preamplifier and TR switch are contained in the magnet leg. The RF amplifier is bolted to the outside of the spectrometer chassis.

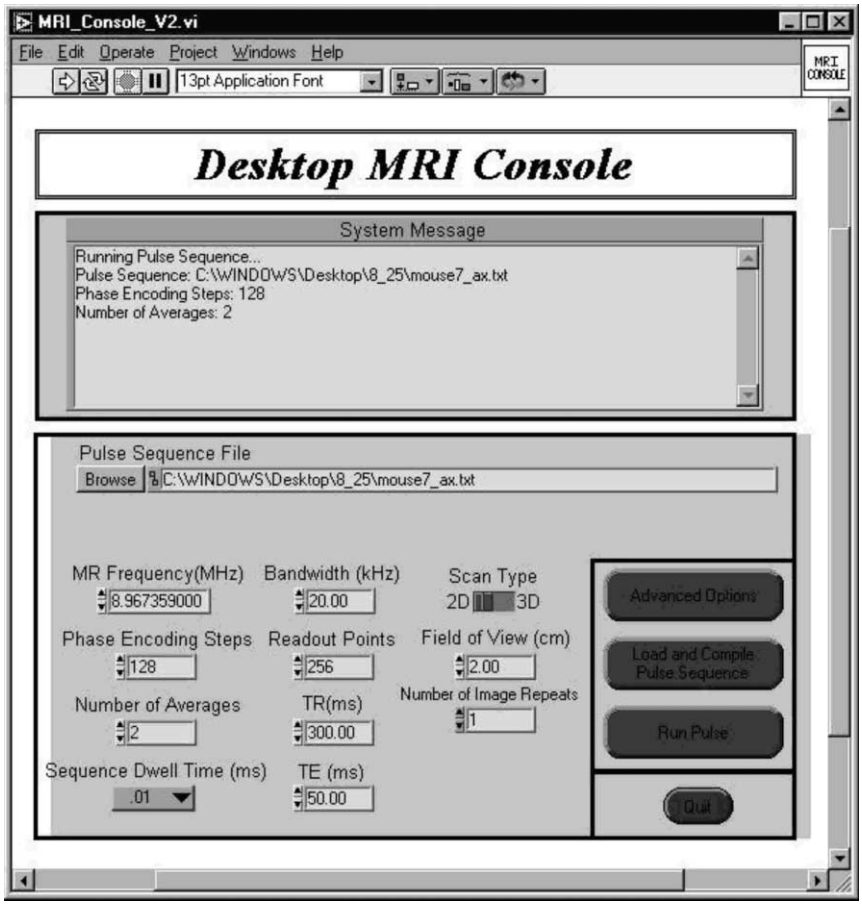

Fig. 5. Control window for the spectrometer software. Additional pop-up windows allow the user control over RF pulse optimization, gradient calibration, spectrometer frequency, and pulse sequence loading.

from 2–300 MHz with a noise figure of less than 1.2 dB. The Miteq amplifier is then followed by a bandpass preselect filter. For smaller samples, additional gain stages are provided by Mini-Circuits (Brooklyn, NY) single chip MAR-6SM amplifiers, specified at 20 dB gain with a 3.0 dB noise figure from DC to 100 MHz.

The I/Q demodulation block was built around an Analog Devices AD607 (Norwood, MA). The AD607 is a two-stage down-conversion receiver on a single chip. The chip accepts RF input frequencies up to 500 MHz and demodulates them down to baseband at the I and Q channel outputs. The chip is available on a populated evaluation board module from the manufacturer. For proper operation, the AD607 evaluation board need only be supplied with two local oscillator signals, an IF gain control voltage, and 3.3–5 volts of DC power. One limitation of this chip is that it has a maximum RF input power level of -15 dBm, however, this was found to be sufficient for small sample imaging.

Following the I/Q demodulation block is a two-channel, audio-band anti-aliasing filter and a two-channel sample-and-hold amplifier. The anti-aliasing filter is based upon Mixed Signal Integration's MSFS2P, a single chip switched capacitor filter (Mixed Signal Integration, San Jose, CA). The MSFS2P has an electronically tunable cutoff frequency (0–20 kHz) and selectable on-chip gains (0, 10 and 20 dB). To enable the use of low-cost digitizer boards, an Analog Devices AD781 single-chip sample-and-hold amplifier was used. The AD781 is capable of 700 ns acquisition times, which makes it possible to simultaneously sample the I and Q channels before they reach the digitizer card. As inexpensive digitizer cards generally multiplex a single A/D, this is important to help minimize timing problems between the I and Q channels.

2.3. Software

The console software was entirely developed in LabVIEW. Because of LabVIEW's graphical nature, it is very easy to design modular code that is both application-specific and user-friendly. These modules can then be brought together to create very complex codes. This allows the rapid development of code for 'push-button' type MR consoles for custom applications, and is ideal for use in an educational environment.

The main console window is shown in Fig. 5. This window allows the user to input imaging parameters such as the number of frequency encoding samples, number of averages, and the repetition rate (TR). The user also supplies the name of the pulse sequence file to be used for imaging. This data is then used to compile the pulse sequence into RAM. Sequence programming is done in a spreadsheet format, with one row for each control line and different columns representing time bins. Each column is assigned a duration in milliseconds. For any given channel, the user has to supply a text-based code for each time slot. These codes determine the type of signal that appears at the output. Options include hard or soft RF waveforms, fixed or ramped gradient amplitudes, and tables for programming phase encode tables or RF phase rotation.

Once the console software reads the sequence, it is compiled into memory. The compiled version is then streamed to the analog output card to provide the necessary timing signals. During image acquisition, the acquisition window is highlighted, as shown in Fig. 6. This window provides a graphical display of the pulse sequence control lines, updated with each phase encode line. Additionally, each echo is displayed. When the sequence is finished, the user is placed in an image analysis window.

3. Results

Benchtop tests measured the bandwidth of the receiver as 1.0 MHz, limited by the IF stage, with a dynamic range of 70 dB, measured using an HP 4195A Network/Spectrum analyzer. Additionally, performance of the spectrometer was evaluated by comparing images obtained from the 0.21 T permanent magnet using a Varian SIS-85 spectrometer to the images obtained using the prototype spectrometer. No significant difference in image quality or SNR was observed in standard 2D spin echo images.

A resolution phantom is shown in Fig. 7a, with dimensions in Fig. 7b. Three-dimensional spin-echo image sets were obtained using this phantom and a mouse fixed in formalin. Figs. 8 and 9 are examples of images obtained with the scanner. Fig. 8 shows two planes from a 3D set with TR/TE = 250/6.2 ms. The upper images are from a data set with a resolution of $128 \times 64 \times 64$, two averages, obtained in 34 min. The lower set has the same resolution but was taken with 12 averages in 3.4 h. Some non-linearity is evident due to the simple gradient and shim designs [17]. Fig. 9 shows 40 axial slices from a 3D set acquired with TR/TE = 250/9.6 ms at $256 \times 128 \times 64$ resolution. The field-of-view was $2.5 \times 2.5 \times 2.5$ cm, and the image has been interpolated to $256 \times 256 \times 64$, giving a displayed reso-

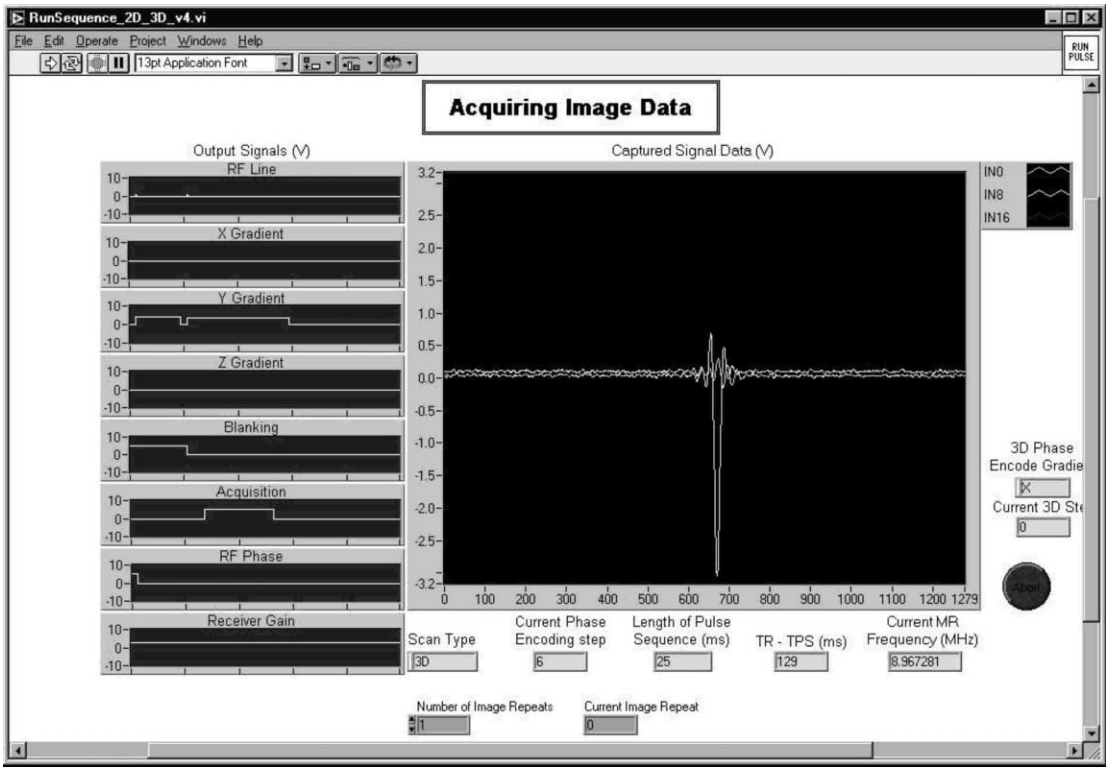

Fig. 6. Image acquisition window. Individual echoes are displayed in real-time. Critical output waveforms, such as gradient and RF blanking, are updated and displayed on the left-hand side of the window with each signal acquisition.

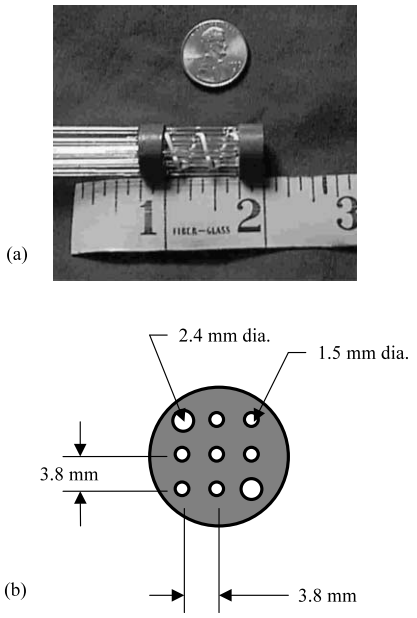

Fig. 7. Photograph of the resolution phantom used to test the desktop imager (a). Tubing is wrapped around four of the posts at a 30° pitch in order to gauge slice thickness. (Tape shown is in inches.) The outer diameter is 0.55 in., and other dimensions are shown in (b).

lution of $100 \times 100 \times 400$ μm. Seen in the figures are the shift in the position of a tubing (insulation from a 24 gauge wire, 37 mils in diameter) wrapped around four of the capillary tubes at a 30° pitch.

Finally, Fig. 10 shows axial and sagital images from a 3D data set on a newborn mouse. The length of the mouse (nose to base of tail) was only 4.5 cm. In each case, TR/TE was 300/9.4 ms with a $2.5 \times 2.5 \times 2.5$ cm field-of-view. The top set (a) was obtained in 20 min, with a resolution of $256 \times 128 \times 16$ and two averages. The middle set (b) was obtained in 8.9 h at $128 \times 128 \times 32$ resolution and 26 averages, and the bottom set (c) required 13.6 h, at $256 \times 128 \times 64$ resolution and 20 averages.

4. Discussion

Although the above results illustrate the ability of the desktop MRI system to produce useable 3D MR data sets in as little as 20 min, clearly longer times will be needed to obtain sufficient SNR for some applications. The permanent magnet frequency is highly dependent on the room temperature, and it was necessary to compensate for the field drift during longer 3D imaging sequences. While a lock could be used, it was found sufficient to simply obtain an echo each time the inner phase encode loop completed and use this echo to recenter the spectrometer frequency. The magnet fre-

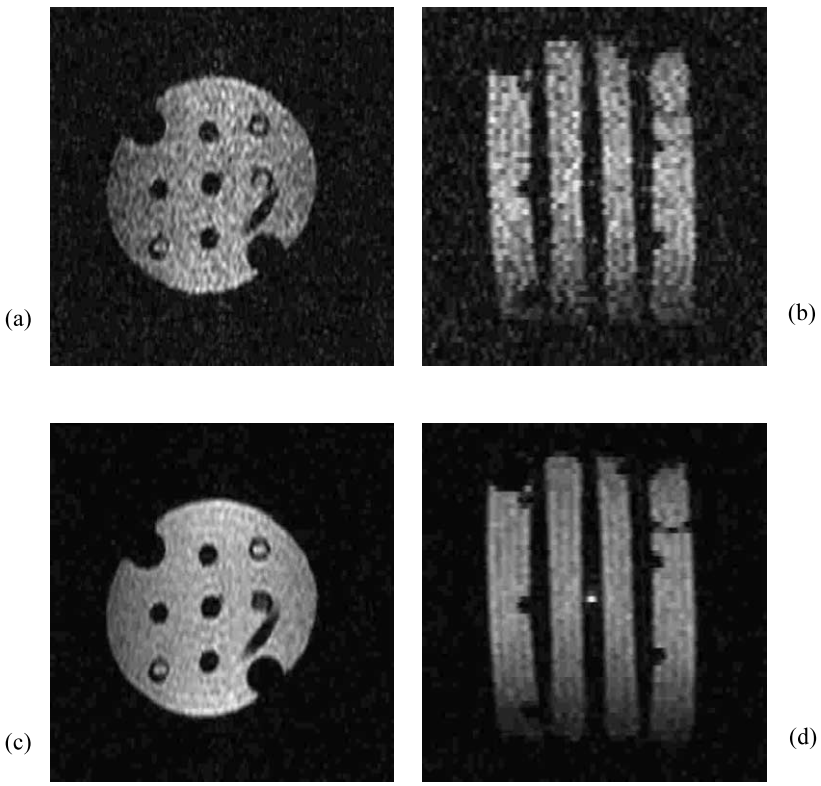

Fig. 8. Axial and sagital images from 3D data sets of the resolution phantom in Fig. 7. TR/TE = 250/6.2 ms, acquired resolution was $128 \times 64 \times 64$, and the field-of-view was $2.5 \times 2.5 \times 3.1$ cm. (a) and (b) (top) were acquired in 32 min, using two averages. (c) and (d) (bottom) were acquired in 3.4 h using 12 averages. All other parameters were identical.

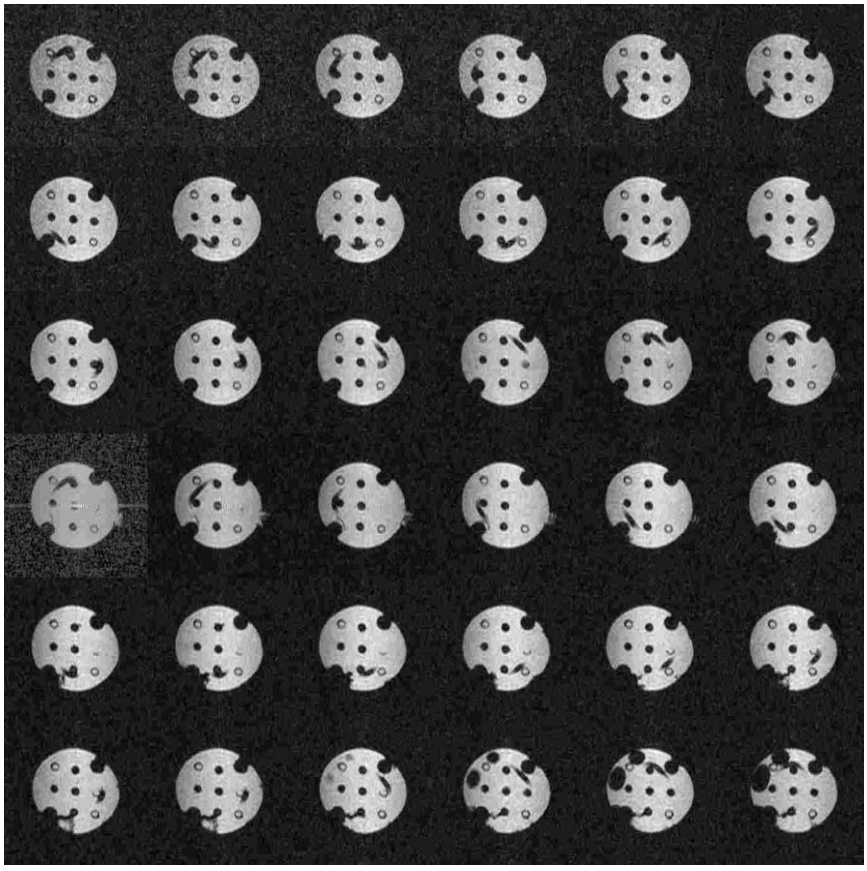

Fig. 9. Thirty-six central slices out of 64 axial slices from the 3D spin echo data set from Fig. 8. Field-of-view was $2.5 \times 2.5 \times 3.1$ cm, with $128 \times 64 \times 64$ resolution, interpolated to $256 \times 256 \times 64$ for a displayed resolution of $100 \times 100 \times 500$ μm. TR/TE = 250/6.2 ms, and 12 averages were acquired for a 3.4 h acquisition time. The spiral wrapped tubing is evident in the images.

quency varied inversely with the pole-face temperature, which followed the room temperature, rising an average of 1.9 °C during the day and cooling during the night. This corresponded to a decrease of 15 kHz in center frequency over the course of a day. The loaded coil Q was under 100 with both the phantom and mouse, giving a coil bandwidth of approximately 90 kHz, far greater than the frequency drift. However, a temperature compensation system or frequency lock will likely be needed if HTS or cooled copper coils are used, due to their higher Q.

Modifications to the system software, such as adding frequency correction, were found to be extremely easy to make due to the flexibility of the LabVIEW programming environment. However, it was found that the overhead associated with the LabVIEW control software has so far restricted the system to repetition times above approximately 200 ms. In the present implementation of the software, the control data for each phase encode line is downloaded during the TR delay after echo acquisition and final gradient pulses, which has led to this minimum delay requirement. Different solutions to this problem are being considered.

The most obvious improvement to the system is the use of cooled copper or high-temperature superconducting RF coils. These coils have the potential to significantly improve the signal-to-noise ratio and reduce the imaging time [18–22], and will likely be necessary to meet the objective of $75 \times 75 \times 200$ μm resolution in practical imaging times.

Further improvements in permanent magnet design, microcoils, and RF integrated circuits promise the development of handheld MR scanners for small fields-of-view, where less gradient and RF power will be required. Small handheld permanent magnets with fields as high as 5 T are being designed for MR microscopy and spectroscopy [23]. A number of groups are working to optimize RF coils for micron resolution MRI and MRS [11,24,25]

5. Conclusions

Desktop MRI systems, such as the one presented in this paper, have the potential to greatly extend the user-base of MR microscopy. The availability of high quality, inexpensive RF components and PC-based in-

strumentation has enabled the development of extremely low-cost and compact MRI systems. For clinical applications, the cost of MRI is warranted by the complexity, but for broader applications, low-cost systems are feasible. For laboratory and classroom applications, the MRI equivalent of the optical microscope appears feasible.

The system presented here, even using standard RF coils, should be sufficient for many imaging applications, such as mice or plants. In the future, techniques such as prepolarized MRI, desktop superconducting magnets, and cryogenic RF coils have the potential to greatly improve the quality of desktop MRI.

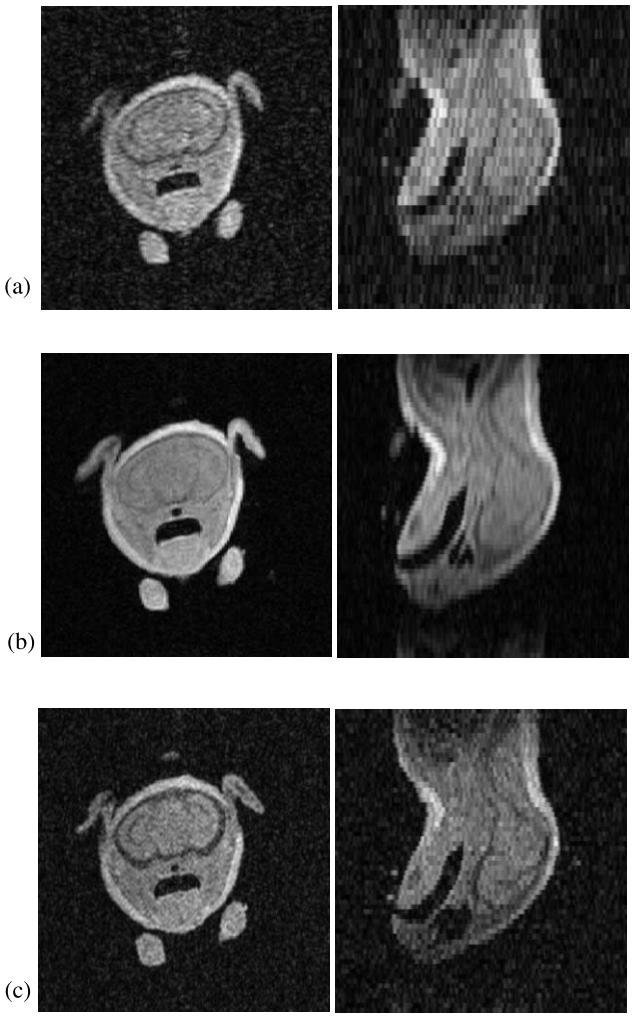

Fig. 10. Axial and sagital images from a 3D data set on a newborn mouse. The length of the mouse (nose to base of tail) was only 4.5 cm. In each case, TR/TE was 300/9.4 ms with a $2.5 \times 2.5 \times 2.5$ cm field-of-view. The top set (a) was obtained in 20 min, with a resolution of $256 \times 128 \times 16$ and two averages. The middle set (b) was obtained in 8.9 h at $128 \times 128 \times 32$ resolution and 26 averages, and the bottom set (c) required 13.6 h, at $256 \times 128 \times 64$ resolution and 20 averages.

Acknowledgements

The authors gratefully acknowledge the support of the Texas Higher Education Coordinating Board grant 000512-0189-1997, as well as IGC, Inc., for the generous donation of the 0.16 T magnet used as a development platform for this research.

References

[1] Balaban RS, Hampshire VA. Challenges in small animal noninvasive imaging. ILAR J 2001;42(3):248–62.
[2] Haishi T, Akita Y, Kose K. MR microscopy of mice at 1.0 Tesla. Proc Int Soc Magn Reson Med 2000;8:1383.
[3] Kose K, Haishi T, Nakanishi A, Okada S, Tsuzaki T. Development of a desktop MR microscope using a small permanent magnet. Proc Int Soc Magn Reson Med 2000;8:1380.
[4] Rokitta M, Rommel E, Zimmerman U, Haase E. A portable NMR imager. Proc ESMRMB 1999;16:528.
[5] Haase A, Rokitta A, Rommel E. NMR portable imager. Proc Int Soc Magn Reson Med. Workshop on MRI Hardware, Cleveland, 23–25 February 2001. p. 23.
[6] Wright SM, Brown DG, Spence DC. NMR Hardware and Desktop Systems. Fourth Mexican Symposium on Medical Physics, vol. 538. American Institute of Physics Conf. Proc. 2000. p. 112–8.
[7] Conolly S et al. Prepolarized magnetic resonance imaging. Proc Int Soc Magn Reson Med. Workshop on MRI Hardware, Cleveland, 23–25 February 2001. p. 22.
[8] Macovski A, Conolly S. Novel approaches to low-cost MRI. Magn Reson Med 1993;30(2):221–30.
[9] Scott G, Xu H, Conolly S, Macovski A. Single conversion image reject receiver for low-field MRI. Proc Int Soc Magn Reson Med 1997;5:60.
[10] Prado PJ, Blumich B, Schmitz U. One-dimensional imaging with a palm-size probe. J Magn Res 2000;144(2):200–6.
[11] Seeber DA. Toward micron resolution proton magnetic resonance imaging of biological cells. Proc. Int. Soc. Magn. Reson. Med. Workshop on MRI Hardware Cleveland, 23–25 February 2001.
[12] Magin RL, Webb AG, Peck TL. Miniature magnetic resonance machines. IEEE Spectrum 1997;34(10):51–61.
[13] Cole DM, Esparza E, Huson FR, Wright SM, Elekes A. Design improvements for permanent magnet-based MRI. Proc Ann Mtg Soc Magn Reson 1997;2:1079.
[14] Esparza E, Cole DM. A low-cost MRI permanent magnet prototype. Second Mexican Symp on Med Physics. American Institute of Physics Conf. Proc. vol. 440, 1998. p. 119–29.
[15] Brown DG, Spence DC, Wright SM. A transceiver for an inexpensive desktop MR microscope. CD-ROM Proc of the World Cong on Med Phys and Biomed Engineering, TH-BA-205-4, 2000.
[16] Thornton J. Instrumentation for low cost, small volume magnetic resonance imaging. Proc Soc Magn Reson Med 1993;12:1315.
[17] Anderson W. Electrical current shims for correcting magnetic fields. Rev Sci Instrum 1961;32(3):241–50.
[18] Black RD, Early TA, Roemer PB, Mueller OM, Mogro-Campero A, Turner LG, et al. A high-temperature superconducting receiver for nuclear magnetic resonance microscopy. Science 1993;259(5096):793–5.
[19] Hurlston SE, Brey WW, Suddarth SA, Johnson GA. A high-temperature superconducting Helmholtz probe for microscopy at 9.4 T. Magn Reson Med 1999;41(5):1032–8.

[20] Miller JR, Hurlston SE, Ma QY, Face DW, Kountz DJ, MacFall JR, et al. Performance of a high-temperature superconducting probe for in vivo microscopy at 2.0 T. Magn Reson Med 1999;41(1):72–9.
[21] van Heteren JG, James TW, Bourne LC. Thin film high temperature superconducting RF coils for low field MRI. Magn Reson Med 1994;32(3):396–400.
[22] Wright AC, Song HK, Wehrli FW. In vivo MR micro imaging with conventional radiofrequency coils cooled to 77 degrees K. Magn Reson Med 2000;43(2):163–9.
[23] Cugat O, Bloch F. The 5 Tesla sphere. http://magnet.ee.umist.ac.uk/reports/P14/p14_2.html.
[24] Peck TL, Magin RL, Kruse J, Feng M. NMR microspectroscopy using 100 microns planar RF coils fabricated on gallium arsenide substrates. IEEE Trans Biomed Eng 1994;41(7):706–9.
[25] Peck TL, Magin RL, Lauterbur PC. Design and analysis of microcoils for NMR microscopy. J Magn Reson B 1995;108(2):114–24.